

## Hot compressive behavior of Ti–3.0Al–3.7Cr–2.0Fe–0.1B titanium alloy

WANG Guo, HUI Song-xiao, YE Wen-jun, MI Xu-jun

State Key Laboratory of Nonferrous Metals and Processes,  
General Research Institute for Nonferrous Metals, Beijing 100088, China

Received 12 October 2011; accepted 14 December 2012

**Abstract:** The hot deformation behavior of Ti–3.0Al–3.7Cr–2.0Fe–0.1B (TACFB) titanium alloy was investigated using a Gleeble-1500D thermal simulator in the temperature range of 800–950 °C, at constant strain rate from 0.01 s<sup>-1</sup> to 10 s<sup>-1</sup> and with height reduction of 70%. Flow stress and microstructure evolution during hot compression of TACFB alloy were investigated. The processing map of TACFB alloy was obtained. The results indicate that the hot deformation behavior of TACFB alloy is sensitive to the deformation temperature and strain rate. The peak flow stress decreases with increasing the test temperature and decreasing the strain rate. The constitutive relationship of TACFB alloy was obtained on the base of Arrhenius equations. When the strain rates are higher than 1.0 s<sup>-1</sup>, the dynamic recrystallization occurs, and the higher the strain rates are, the more the recrystallization is.

**Key words:** titanium alloy; Ti–3.0Al–3.7Cr–2.0Fe–0.1B alloy; hot compressive; constitutive relationship; processing map; dynamic recrystallization

### 1 Introduction

Titanium and titanium alloys are being considered as candidates in civil fields due to their high specific strength, half elastic modulus of steel, non-magnetic, low thermal expansion coefficient, excellent fatigue and crack-propagation behavior, good manufacturability and no pollution to environment [1,2]. For these advantages, titanium alloys have been attracting scientists' attention as automobile materials. As vehicle material, it will reduce the mass of the car, reduce fuel consumption, raise efficiency, improve the environment and reduce noise [3,4].

But the cost of titanium alloys is much higher than that of steel and aluminum alloys which are used widely in civil. The high cost hinders the application of titanium alloys in civil fields which are very sensitive to money, and the automotive industry is a typical example [5]. So, how to reduce the cost of titanium alloys have become the hot topic and the key point. At present, there are about three successful methods to reduce the cost of titanium alloys [6–8]: 1) take advantage of cheaper raw materials to design alloy, such as Mo–Fe master alloy, Fe element etc; 2) improve the material processing

characteristics; and 3) enhance the material utilization ratio during the material processing.

Ti–3.0Al–3.7Cr–2.0Fe–0.1B (TACFB) is kind of low cost titanium alloy developed by ourselves. The low cost Cr–Fe master alloy, Fe and elements were used to design the new type TACFB alloy, and the alloy was developed for the automobile spring in civil fields on the original purpose. In order to learn the processing performance of the alloy, the thermal simulation compression tests of TACFB alloy were carried out.

Many factors could influence the compressive behavior of metal materials during hot working, such as deformation temperature, strain rate and deformation degree. And the constitutive equation of material could express the relationship among the deformation temperature, flow stress and strain rate. DU et al [9] studied the hot deformation behavior and constitutive equation of Ti26 alloy. They got the flow stress data at various temperatures and strain rates, calculated the deformation activation energy and established the constitutive equation. The results showed that the main softening mechanism is dynamic recovery in  $\beta$  phase region. LIU et al [10] studied the hot deformation behavior of Ti–6.5Al–3.5Mo–1.5Zr–0.3Si alloy with acicular microstructure, considered the effect of different

microstructure on the deformation behavior and made the processing map. The results showed that in the two regions a peak stress exhibited followed by continuous flow softening; whereas the flow stress attained a steady state regime in  $\beta$  region. Thus, this work will introduce the hot deformation behavior of TACFB alloy. In this work, the deformation temperature and strain rates which influence the stress are considered, and then the constitutive equation and the processing map are established, and the microstructure evolution is observed.

## 2 Experimental

### 2.1 Material

The TACFB alloy was double melted by consumable vacuum arc remelting (VAR) process. The finished ingots were processed into bars of 12 mm in diameter with two steps. The ingots was initially break down in  $\beta$  phase field around 1050 °C followed by hot rolling in  $\alpha+\beta$  field. The chemical composition of TACFB alloy is listed in Table 1. The  $\beta$  transformation temperature of TACFB alloy is (885±5) °C. The original microstructure of the bar of TACFB alloy is shown in Fig. 1.

**Table 1** Chemical composition of Ti–3.0Al–3.7Cr–2.0Fe–0.1B alloy (mass fraction, %)

Al	Cr	Fe	B	Si	Ti
2.9–3.1	3.6–3.8	1.9–2.1	0.1	0.06–0.07	Bal.

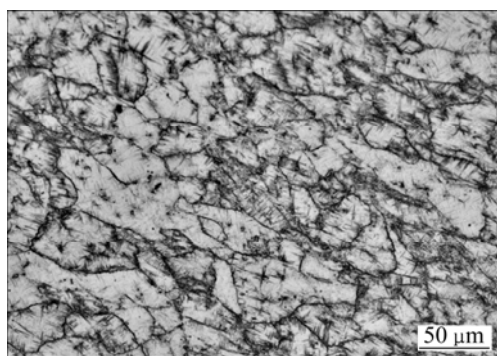


**Fig. 1** Original microstructure of Ti–3.0Al–3.7Cr–2.0Fe–0.1B alloy

### 2.2 Compression tests

The cylindrical thermal simulation compression specimens of 8 mm in diameter and 12 mm in height were machined from the bar along the axial direction. Hot compression tests were carried out on the specimens with the strain rates from 0.01 s<sup>-1</sup> to 10 s<sup>-1</sup> and temperature from 800 °C to 950 °C. The experiments were carried out on the Gleeble-1500D thermal simulation test machine. Thermocouples welded in the middle surface of the specimens were used to measure

the actual temperature of the specimens during experiments. In order to reduce the effect of friction during the tests, proper lubricant of graphite pieces was used. The specimens were compressed to 70% of height. Figure 2 shows the hot deformation process.

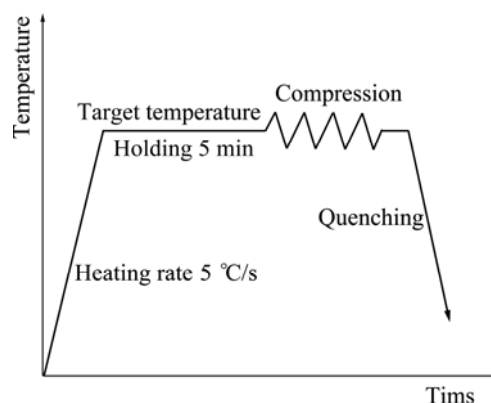


**Fig. 2** Schematic diagram of hot deformation

### 2.3 Microstructure observation

The deformation microstructure was observed after tests. The specimens were cut into two parts along the axial direction by wire cutting. One part was used as the metallographic specimen. The metallographic specimens were corroded using the solution containing 10% HF, 3% HNO<sub>3</sub> and 96% H<sub>2</sub>O. And the microstructure was observed by the metallurgical microscope.

## 3 Results and discussion

### 3.1 True stress—true strain curves

The typical true stress—true strain curves obtained at various temperatures and strain rates are presented in Fig. 3. The curves show that the flow stress behavior of TACFB alloy is sensitive to strain rates and deformation temperature. In Fig. 3, the true stress increased quickly with increasing the true strain at the initial phase and then arrived at a peak stress. In general, after the peak stress, the true stress decreased gradually with increasing the true strain, and then tended to a steady state.

Figure 3 indicates that the strain hardening was greater than the dynamic recovery or dynamic recrystallization softening process, therefore the stress increased rapidly with the strain ascending in the early stage of deformation. The flow stress would reach a peak value, when the hardening and softening process were approximately equal. After the peak flow stress, the strain hardening is less than the dynamic recovery or dynamic recrystallization softening, which could cause the flow stress decreasing gradually with increasing the strain. Then, with the deformation continuing, the true stress almost remained constant [10–12]. But at high strain rate of 10 s<sup>-1</sup>, when the deformation temperature

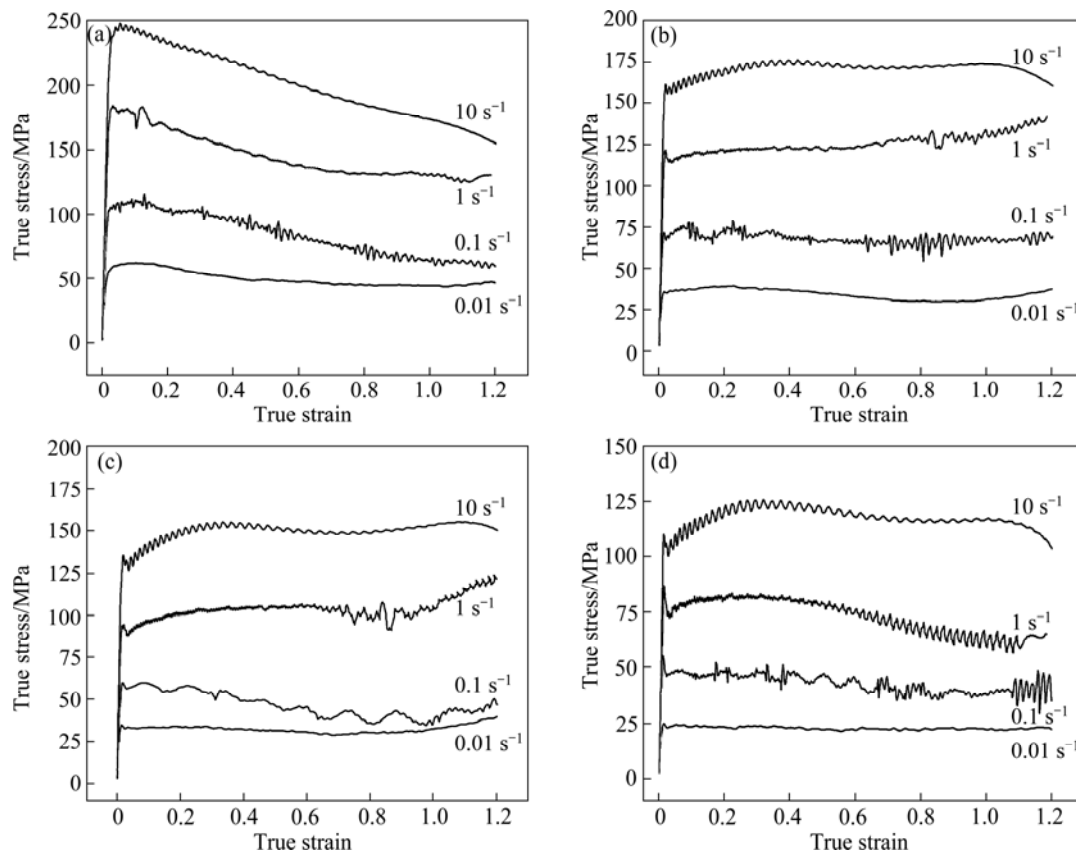


**Fig. 3** True stress—true strain curves of Ti-3.0Al-3.7Cr-2.0Fe-0.1B alloy at different temperatures: (a) 800 °C; (b) 850 °C; (c) 900 °C; (d) 950 °C

were 850, 900 and 950 °C, after peak stress, the strain hardening was a little higher than the dynamic recovery or dynamic recrystallization softening process.

In addition, when the temperature was 800 °C and the strain rates were  $10 \text{ s}^{-1}$  and  $0.01 \text{ s}^{-1}$ , the peak flow stresses were 248.1 MPa and 62.18 MPa, respectively, the difference was 185.92 MPa; at 950 °C, the peak flow stress are 125.7 MPa and 24.83 MPa, respectively, and the difference was 100.87 MPa. It is shown that at a given temperature, the larger the strain rate is, the larger the peak stress is. The flow stress as a function of temperature and strain rate is given in Table 2. There may be several reasons to interpret this situation. Firstly, the plastic deformation rises with ascending the strain rates, which would emerge the amount of dislocation in alloy, drive lots of dislocation movement at the same time and prompt the aggravating distortion. Secondly, the dislocation movement speeds up with the increase of strain rates, therefore more shear stress would be needed, and the critical shear stresses ascend in the inner of metal. Finally, due to the increasing of strain rates, the dynamic recovery or dynamic recrystallization could not supply in time and in sufficient, consequently the stress increases with increasing the strain rates [12,13].

Figure 4 shows the flow stress changes with the

**Table 2** Variation of peak flow stress

Strain rate/ $\text{s}^{-1}$	Peak flow stress/MPa			
	800 °C	850 °C	900 °C	950 °C
0.01	62.18	39.41	39.94	24.83
0.1	107.55	78.56	60.07	55.10
1.0	184.04	141.79	123.91	87.06
10.0	248.10	176.46	155.35	125.70

deformation temperature. The peak stress decreased gradually with increasing the temperature. This is mainly due to the fact that the material deformation resistance decreases with increasing the deformation temperature, viz the heat activation is enhanced with increasing the temperature, and the critical resolved shear stress is decreased with increasing the temperature. And the dynamic recovery or dynamic recrystallization becomes easier, accordingly the density of dislocation decreases; therefore the flow stress decreases with increasing the temperature [14].

### 3.2 Kinetic analysis

The flow stress of thermal deformation is concerned with deformation, strain rate and deformation temperature. The high temperature deformation of

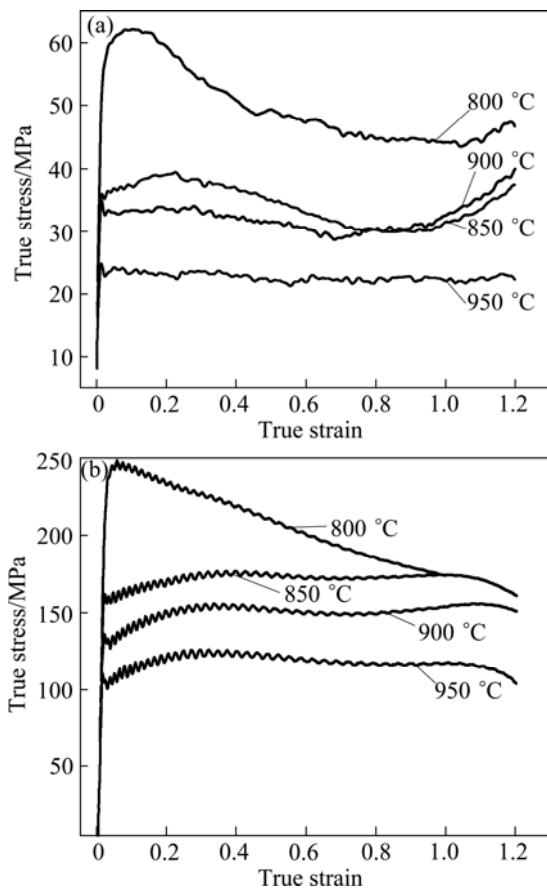


Fig. 4 Effect of temperature on true stress—true strain at different strain rates: (a)  $1.0 \text{ s}^{-1}$ ; (b)  $10 \text{ s}^{-1}$

metal is a thermal activation process, which is affected by the deformation temperature, strain rate and other factors. This process could be described by Arrhenius hyperbolic sine constitutive relationship [9,12].

The steady state equation for hot deformation relates flow stress with temperature and strain rates as

$$\dot{\epsilon} = A[\sinh(\alpha\sigma)]^n \exp\left(-\frac{Q}{RT}\right) \quad (1)$$

And it can be expressed as

$$Z = A[\sinh(\alpha\sigma)]^n = \dot{\epsilon} \exp\left(\frac{Q}{RT}\right) \quad (2)$$

where  $\sigma$  is the flow stress;  $\dot{\epsilon}$  is the strain rate;  $R$  is the gas constant ( $8.314 \text{ J}\cdot\text{mol}^{-1}\cdot\text{K}^{-1}$ );  $A$  is the material constant;  $T$  is the temperature in Kelvin;  $n$  is the stress exponent;  $Q$  is the deformation activation energy;  $Z$  is a Zener-Hollomon parameter, whose physical meaning is the temperature compensated strain rate.

For the relationship between the flow stress and strain rate, when the flow stress is low,

$$\dot{\epsilon} = A_1\sigma^{n_1} \exp\left(-\frac{Q}{RT}\right) \quad (3)$$

and when the flow stress is high,

$$\dot{\epsilon} = A_2 \exp(\beta\sigma) \exp\left(-\frac{Q}{RT}\right) \quad (4)$$

where  $A_1$ ,  $A_2$ ,  $n_1$  and  $\beta$  are constants. The relationship among  $\alpha$ ,  $\beta$  and  $n_1$  is

$$\alpha = \beta/n_1 \quad (5)$$

Using Eq. (3), or Eq. (4) and Eq. (5) the parameters in Eq. (1) can be gotten. Taking logarithm for Eq. (3) and Eq. (4) yields

$$\ln \sigma = \frac{\ln \dot{\epsilon}}{n_1} - \frac{\ln A_1}{n_1} \quad (6)$$

$$\sigma = \frac{\ln \dot{\epsilon}}{\beta} - \frac{\ln A_2}{\beta} \quad (7)$$

According to the true stress—true strain curves, we could get the curves of  $\ln \sigma - \ln \dot{\epsilon}$  when the stress is low and  $\sigma - \ln \dot{\epsilon}$  when the stress is high as shown in Fig. 5. By using least square method for linear regression, from Fig. 5 the values of  $n_1$  (4.640113) and  $\beta$  (0.052454) are obtained. Then taking the values into Eq. (5) and the value of  $\alpha$  (0.0113) is gotten.

If the activation energy  $Q$  does not change with deformation temperature  $T$ , Eq. (1) takes into logarithm form as

$$\ln \dot{\epsilon} = \ln A + n \ln[\sinh(\alpha\sigma)] - \frac{Q}{RT} \quad (8)$$

Then, the following equation is gotten.

$$Q = R \left[ \frac{\partial \ln \dot{\epsilon}}{\partial \ln[\sinh(\alpha\sigma)]} \right]_T \left[ \frac{\partial \ln[\sinh(\alpha\sigma)]}{\partial (1/T)} \right]_{\dot{\epsilon}} \quad (9)$$

According to the value of  $\alpha$  and true stress—true strain curves, the relationships  $\ln[\sinh(\alpha\sigma)] - \ln \dot{\epsilon}$  and  $\ln[\sinh(\alpha\sigma)] - T^{-1}$  are shown in Fig. 6. The value of  $n$  can be calculated from Fig. 6, which is equal to 3.348963. Then, taking the value into Eq. (8) and Eq. (9), we can acquire the  $Q$  ( $261.7198 \text{ kJ}\cdot\text{mol}^{-1}$ ) and  $A$  ( $6.1 \times 10^{12}$ ) values.

Taking  $Q$  into Eq. (2) could get the relation  $Z = \dot{\epsilon} \times \exp(261719.8/RT)$ . Taking the different strain rates into Eq. (2) could acquire the different values of  $Z$  under different temperatures.

According to the values of  $Z$  and the peak stresses, the relationship between  $\ln Z$  and  $\ln[\sinh(\alpha\sigma)]$  can be gotten, which is shown in Fig. 7. Using the linear regression the linear relationship between  $\ln Z$  and  $\ln[\sinh(\alpha\sigma)]$  can be gotten as  $\ln Z = 3.11374 \ln[\sinh(\alpha\sigma)] + 20.41741$ , and the correlation coefficient is as high as 0.972. On the base of these values of different parameters, we could get the constitutive equation as  $\dot{\epsilon} = 6.1 \times 10^{12} [\sinh(0.0113\sigma)]^{3.35} \exp(-261719.8/RT)$ .

### 3.3 Processing map

The processing map of the TACFB alloy has been

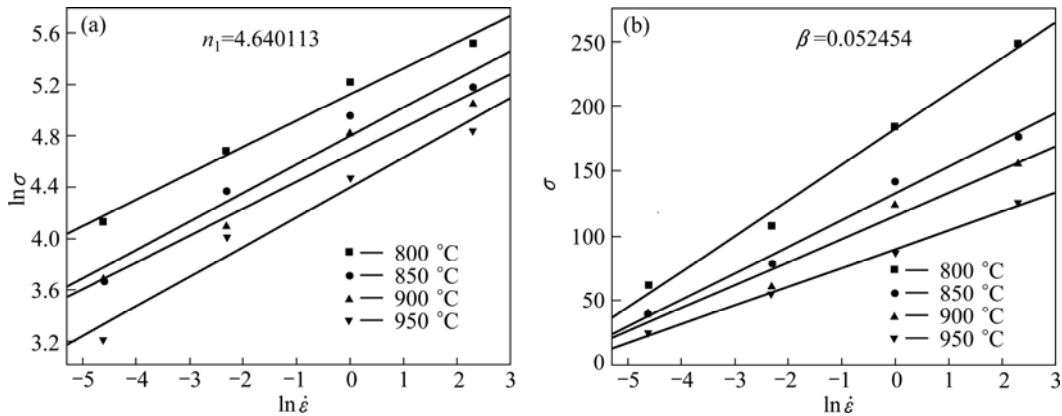


Fig. 5 Relationships between strain rates and peak-stress: (a)  $\ln\sigma - \ln\dot{\epsilon}$ ; (b)  $\sigma - \ln\dot{\epsilon}$

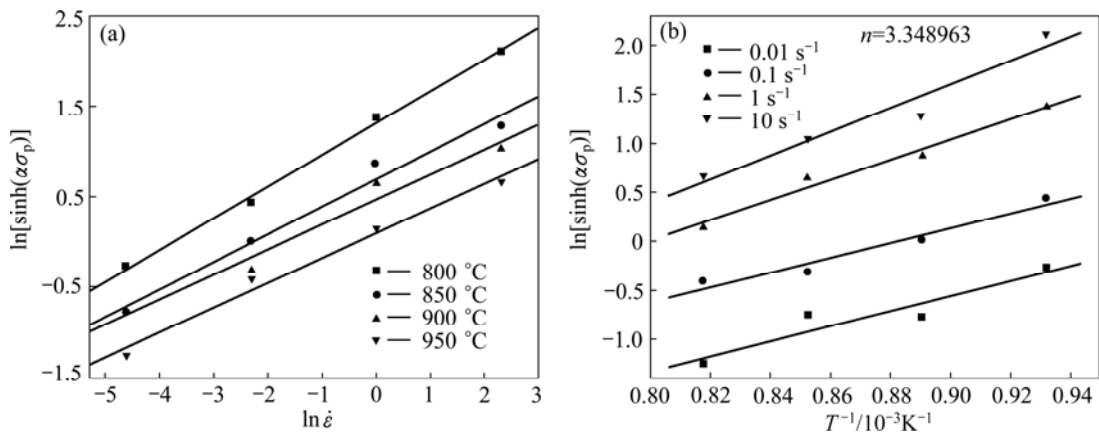


Fig. 6 Relationships between peak-stress and deformation temperature: (a)  $\ln[\sinh(\alpha\sigma_p)] - \ln\dot{\epsilon}$ ; (b)  $\ln[\sinh(\alpha\sigma_p)] - 1000/T$

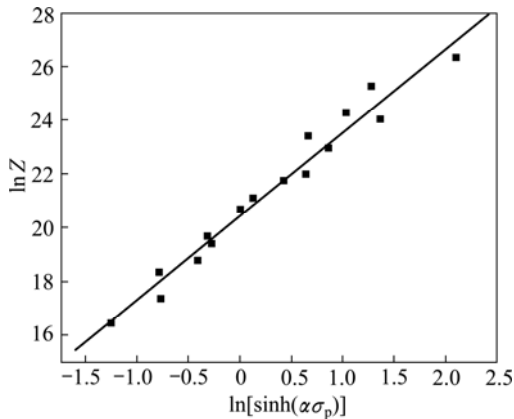


Fig. 7 Relationship between flow stress and Zener-Hollomon parameter

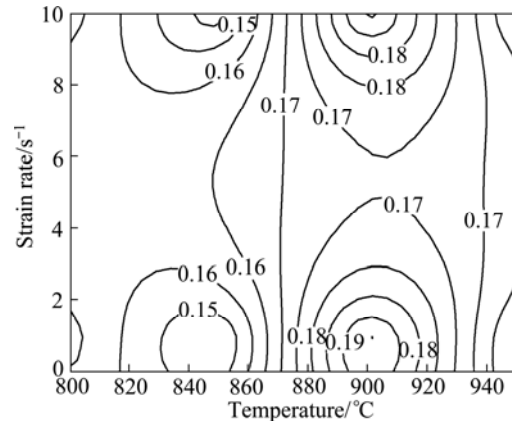


Fig. 8 Processing map of Ti-3.0Al-3.7Cr-2.0Fe-0.1B alloy ( $\epsilon=0.7$ )

established through the method suggested by PRASAD [15]. The processing map is shown in Fig. 8. The isoline shows the energy dissipation factor, and the digital is the numerical value. There is no processing instability area under these conditions in this work. This may be because the temperature and strain rates scope are not broad enough. When the temperature is nearly 900 °C, the strain rate ranges from 0.01 s<sup>-1</sup> to 1.0 s<sup>-1</sup> and could reach 0.19. Some researchers pointed out that when the strain rate is lower, the energy dissipation efficiency of

dynamic recrystallization is higher for higher stacking fault energy metal. For higher stacking fault energy titanium, when the temperature is above the phase transformation temperature, the strain rate is lower, the energy dissipation is higher, and there would occur some dynamic recrystallization grain.

3.4 Microstructure observation

The microstructures of the specimens deformed at temperature of 900 °C are presented in Fig. 9. For

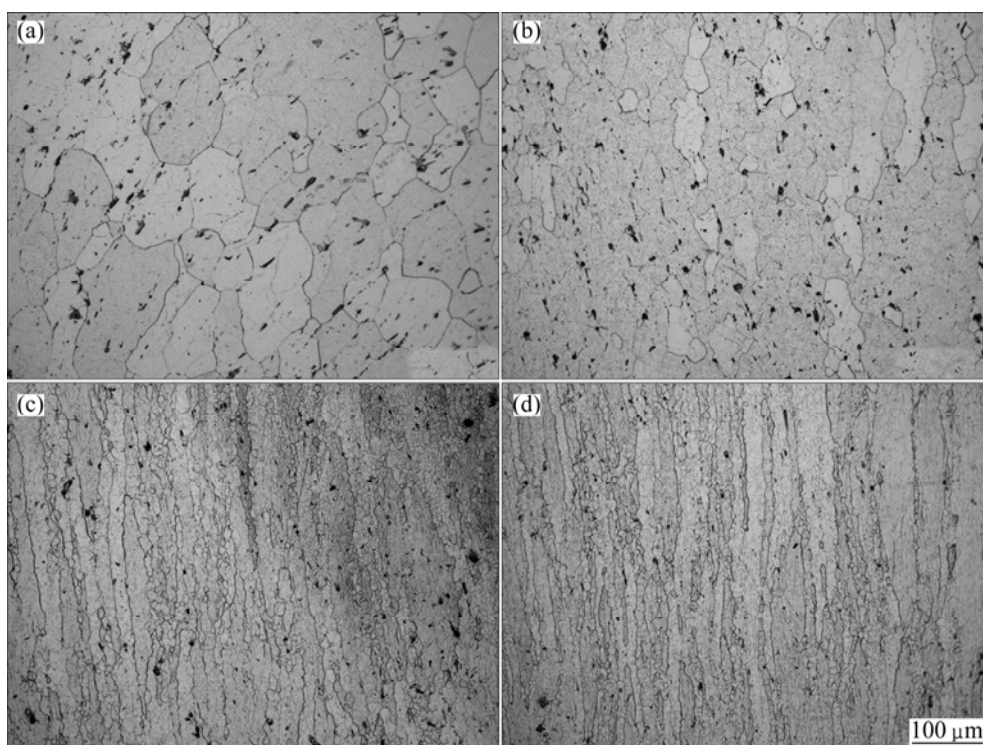


**Fig. 9** Microstructures of Ti-3.0Al-3.7Cr-2.0Fe-0.1B alloy deformed under different strain rates: (a)  $0.01 \text{ s}^{-1}$ ; (b)  $0.1 \text{ s}^{-1}$ ; (c)  $1.0 \text{ s}^{-1}$ ; (d)  $10 \text{ s}^{-1}$

titanium alloys recovery and recrystallization would occur because  $\alpha$  and  $\beta$  phase have a chance to deform in the two phase region. But the  $\beta$  phase is of BCC structure; and the slip system of this structure is easy to move as compared with the HCP structure of titanium alloys. Thus, there are more recovery and recrystallization.

Figure 9 indicates that the inner grains of alloy elongate along the vertical direction of compression. When the strain rate is less than  $0.1 \text{ s}^{-1}$ , the  $\beta$  grains are elongated, therefore the deformation of the alloy is mainly dynamic recovery. When the strain rate is higher than  $1.0 \text{ s}^{-1}$ , there would produce tiny recrystallization grains along the  $\beta$  grain boundary, and the recrystallization nucleation rate increases with increasing the deformation. Hence, the dynamic recrystallization phenomenon is more obvious with rising the strain rates, and the incomplete recrystallization would occur during the deformation process. The grain size is finer at higher strain rates.

## 4 Conclusions

1) The influence of temperature and strain rate is obvious for the hot compression deformation behavior of TACFB alloy. The peak flow stress decreases with the increase of temperature and decrease of strain rates.

2) According to the Arrhenius equation, the constitutive equation of Ti-3.0Al-3.7Cr-2.0Fe-0.1B

alloy was constructed. The constitutive equation is  $\dot{\epsilon} = 6.1 \times 10^{12} [\sinh(0.0113\sigma)]^{3.35} \exp(-261719.8/RT)$ .

3) The processing map indicates that the energy dissipation is high as the strain rate is low. When the strain rates are larger than  $1.0 \text{ s}^{-1}$ , the dynamic recrystallization occurs in the alloy. The recrystallization is more evident as the strain rate is higher.

## References

- [1] LEYENS C, PETERS M. Titanium and titanium alloys: Fundamentals and applications [M]. Germany: Wiley-VCH, 2003: 3.
- [2] BAREL E, HAMU G B, ELIEZER D, WAGNER L. The effect of heat treatment and HCF performance on hydrogen trapping mechanism in Ti metal LCB alloy [J]. J Alloy Compd, 2009 468: 77–86.
- [3] HARTMAN A D, GERDEMANN S J, HANSEN J S. Producing lower-cost titanium for automotive applications [J]. JOM, 1998, 50(9): 16–19.
- [4] FUJII H, TAKAHASHI K, YAMASHITA Y. Application of titanium and its alloys for automobile parts [J]. Shinnittetsu Giho, 2003, 378: 62–67.
- [5] FALLER K, FROES F H. The use of titanium in family automobiles: Current trends [J]. JOM, 2001, 53(4): 27–29.
- [6] LI Z, SUN JK. Development and applications of low cost titanium alloys [J]. Rare Met Mater Eng, 2008, 37(z3): 973–976. (in Chinese)
- [7] KAWABE Y. Research activities on cost effective metallurgy of titanium alloys in Japan [C]// GRINNING I V. Proc of 9th World Conference on Titanium. Russia: Central Research Institute of Structural Materials Prometey, 1999, 1: 1275–1282.
- [8] ESTEBAN P G, RUIZ-NAVAS E M, BOLZON L. Low-cost titanium alloys? Iron may hold the answers [J]. Met Powder Rep, 2008, 63:

- 24–27.
- [9] DU Y, QI Y L, ZHAO Y Q, WANG R N, LIU W, XI Z P, HONG Q. Hot deformation behavior and constitutive equations of titanium alloy Ti26 [J]. Transactions of Nonferrous Metals Society of China, 2007, 17: s500–s503.
- [10] LIU G F, ZHANG S Z, CHEN L Q. Hot deformation behavior of Ti–6.5Al–3.5Mo–1.5Zr–0.3Si alloy with acicular microstructure [J]. J Cent South Univ Technol, 2011, 18(2): 296–302.
- [11] SUN S D, ZONG Y Y, SHAN D B, GUO B. Hot deformation behavior and microstructure evolution of TC4 titanium alloy [J]. Transactions of Nonferrous Metals Society of China, 2010, 20: 2181–2184.
- [12] BALASUBRAHMANYAM V V, PRASAD Y V R K. Deformation behavior of beta titanium alloy Ti–10V–4.5Fe–1.5Al in hot upset forging [J]. Mater Sci Eng A, 2002, 336: 150–158.
- [13] LIU Z E. Material science [M]. Xi'an: Northwestern Polytechnical University Press, 2003: 273. (in Chinese)
- [14] GUO A H, YU W, ZHANG Y Q, ZHU Y S. Hot deformation behaviors of biomedical  $\beta$ -Ti30Nb13Zr0.5Fe alloy [J]. The Chinese Journal of Nonferrous Metals, 2010, 20(S1): 357–364. (in Chinese)
- [15] PRASAD Y V R K, SESHACHARYULU T. Processing maps for hot working of titanium alloys [J]. Mater Sci Eng A, 1998, 243(1–2): 82–88.

## Ti–3.0Al–3.7Cr–2.0Fe–0.1B 钛合金的热压缩行为

王 国, 惠松晓, 叶文君, 米绪军

北京有色金属研究总院 有色金属材料制备加工国家重点实验室, 北京 100088

**摘 要:** 利用 Gleeble-1 500D 热模拟试验机对低成本钛合金 Ti–3.0Al–3.7Cr–2.0Fe–0.1B 的热压缩行为进行研究。采用的应变速率分别为 0.01、0.1、1.0 和  $10\text{ s}^{-1}$ , 选用的温度分别为 800、850、900 和 950 °C, 试样的变形量最大为 70%。结果表明: 峰值流变应力随着温度的增加和应变速率的降低而降低; 根据 Arrhenius 公式获得该合金在本实验条件下的本构方程为  $\dot{\epsilon} = 6.1 \times 10^{12} [\sinh(0.0113044\sigma)]^{3.35} \exp(-261719.8/RT)$ , 并得到了该合金的加工图。当应变速率大于等于  $1.0\text{ s}^{-1}$  时, 合金内发生动态再结晶现象, 且应变速率越大动态再结晶现象越明显。

**关键词:** 钛合金; Ti–3.0Al–3.7Cr–2.0Fe–0.1B 合金; 热压缩; 本构关系; 加工图; 动态再结晶

(Edited by YUAN Sai-qian)